



Observations of the convective environment in developing and non-developing tropical disturbances

Roger K. Smith^a and Michael T. Montgomery^b

^a *Meteorological Institute, University of Munich, Munich, Germany*

^b *Dept. of Meteorology, Naval Postgraduate School, Monterey, CA & NOAA's Hurricane Research Division, Miami, FL, USA.*

Abstract:

Analyses of thermodynamic data gathered from airborne dropwindsondes released from the upper troposphere during the Pre-Depression Investigation of Cloud Systems in the Tropics (PREDICT) experiment are presented. The main focus is on two systems that finally became Hurricanes Karl and Matthew and one system that attained Tropical Storm status (Gaston), but subsequently weakened and never redeveloped during five days of monitoring. Data for all events show that the largest values of total precipitable water are collocated with the surface trough and with values of convective available potential energy that seem high enough to support convective organization. These values coincide mostly with low values of convective inhibition. Vertical profiles of virtual potential temperature show little variability between soundings on a particular day, but the system means from day to day show a slight warming. In contrast, vertical profiles of pseudo-equivalent potential temperature, θ_e , show much more variability between soundings on a particular day on account of the variability in moisture.

In all systems, there is a tendency for the lower troposphere to moisten, but in the non-developing system, the middle and upper troposphere became progressively drier during the five days of observations. In the developing systems, the upper levels moistened. The most prominent difference between the non-developing system and the two systems that developed was the much larger reduction of θ_e between the surface and a height of 3 km, typically 25 K in the non-developing system, compared with only 17 K in the systems that developed. Conventional wisdom would suggest that, for this reason, the convective downdraughts would be stronger in the non-developing system and would thereby act to suppress the development. Here we propose an alternative hypothesis in which the drier mid-level air weakens the convective updraughts and thereby the convective amplification of absolute vorticity necessary for development.

Copyright © 2011 Royal Meteorological Society

KEY WORDS Tropical cyclogenesis, formation, spin-up, intensification, PREDICT, GRIP, IFEX

Received October 17, 2011; Revised ; Accepted

1 Introduction

Understanding the dynamics of tropical cyclogenesis remains one of the great unsolved problems in tropical meteorology. One reason for the lack of understanding is undoubtedly the fact that genesis occurs over the tropical oceans where conventional observational data such as radar data, radiosonde soundings and surface data are relatively sparse. While there have been a few field experiments directed at documenting cyclogenesis (Bister and Emanuel 1997, Ritchie and Holland 1999, Halverson *et al.* 2007, Elsberry and Harr 2008 and Zipser *et al.* 2009) and a few serendipitous sets of measurements (Reasor *et al.* 2005, Houze *et al.* 2009), many questions remain about the processes involved and their relative importance. A recent review of work over the past few years is given by Montgomery and Smith (2010).

In the late summer of 2010, a trio of field experiments was conducted by the National Aeronautics and Space Administration (NASA), National Oceanic and

Atmospheric Administration (NOAA) and National Science Foundation (NSF) to investigate tropical cyclogenesis in the Caribbean and West Atlantic and the subsequent intensification of storms in these regions. While two of the experiments¹ included intensification in their portfolio of objectives, the Pre-Depression Investigation of Cloud Systems in the Tropics (PREDICT) experiment was designed exclusively to study genesis. Priority was given to developing storms prior to their classification as tropical depressions as defined by forecasters², even when

¹The Genesis and Rapid Intensification Processes (GRIP) project of NASA and the Intensity Forecasting Experiment (IFEX) of the NOAA.

²The glossary on the NOAA Hurricane Research Division website uses “tropical cyclone as the generic term for a nonfrontal synoptic-scale low-pressure system over tropical or sub-tropical waters with organized convection (i.e. thunderstorm activity) and a definite cyclonic surface wind circulation.” Notably, this definition does not invoke any wind threshold. The same glossary defines a “tropical depression as a tropical cyclone with maximum sustained surface winds of less than 17 m s^{-1} (34 kt, 39 mph) and, in the Atlantic and Eastern Pacific Basins, a tropical storm as a tropical cyclone with surface winds between 17 m s^{-1} and 33 m s^{-1} .” In this study we will define genesis as the formation of a tropical depression and we impose no formal threshold on wind speed.

¹Correspondence to: Prof. Roger K. Smith, Meteorological Institute, Ludwig-Maximilians University of Munich, Theresienstr. 37, 80333 Munich, Germany. E-mail: roger.smith@lmu.de



mature storms were present nearby. The primary measurement platform of PREDICT was the National Center for Atmospheric Research (NCAR) GV research aircraft, equipped with dropsondes and onboard sensors for meteorological variables and ice microphysics. The range and speed of the GV, and the high altitude ($\approx 13\text{--}14$ km) from which it could release dropsondes, were exploited to sample storm formation from Central America to the mid-Atlantic (roughly 40°W) operating out of St. Croix in the U.S. Virgin Islands. Some measurements were made also by the NASA DC8 research aircraft, which, has the capability to release dropsondes from moderately high in the troposphere ($\approx 10\text{--}11$ km).

The PREDICT field experiment aimed to gather data on developing and non-developing tropical disturbances and to test the recently proposed marsupial model of tropical cyclogenesis in association with tropical easterly waves (Dunkerton *et al.* 2009). The overarching hypothesis was that tropical depression formation is greatly favoured in the critical-layer region of the synoptic-scale, pre-depression wave or subtropical disturbance. A summary of the scientific basis for the experiment as well as some highlights of the data obtained is described by Montgomery *et al.* (2011). The experiment collected, *inter alia*, unprecedented³ dropwindsonde data from two high-altitude flying aircraft (the NCAR GV and NASA DC8). When these aircraft were flying the same system, the flights were staggered in time to provide an optimum temporal coverage. The flights were focused on the so-called “wave pouch” (Dunkerton *et al.* 2009) and its immediate vicinity. The wave pouch is defined as the region of recirculating streamlines depicted in the frame of reference at a given altitude moving with the tropical disturbance in the lower troposphere and the centre of circulation is referred to as the “sweet spot”, the location at which, according to the marsupial paradigm, a tropical cyclone is most likely to form. In the PREDICT experiment, the 700 mb level was typically used to track the pouch of a candidate disturbance and to delineate its boundary with environmental air. These data provide a unique opportunity to examine the evolution of the thermodynamic and kinematic structure of the wave pouches identified for both developing and non-developing systems.

In this study we will examine thermodynamic aspects of the sounding data acquired during the experiment, focusing on the day-to-day changes in the mean profiles of potential temperature and equivalent potential temperature. While these analyses cannot directly offer an understanding of the spin up process on the mesoscale, they nonetheless offer quantitative information on the changes in the thermodynamic mean states during development or non-development, such as the stabilization or otherwise of the mean sounding and the moistening of the mean sounding during the evolution of the disturbance.

³In the TCS08 experiment, the US Air Force C-130 aircraft was flown at a relatively high altitude of approximately 9 km in conjunction with the Naval Research Laboratory P-3 with the ELDORA radar and Doppler wind lidar on board. However during the experiments before TCS08, flight altitudes were limited to a few kilometres.

The outline of this paper is as follows. Section 2 details the events discussed and section 3 describes the dropwindsonde data and methods of analysis. Section 4 presents the results of the analyses for each storm. The results are discussed in section 5 and the conclusions are given in section 6.

2 Events discussed

The storms sampled by PREDICT aircraft missions are summarized by Montgomery *et al.* (2011, see their Table 1). These storms were fairly evenly split between developing and non-developing systems. While some cases had a high potential for genesis from the time of the first GV flight into them and subsequently developed, one system departed from this pattern. Gaston was a surprising instance where development occurred initially, but following a period of decline (sampled by the GV) re-development did not occur. Matthew surprisingly formed in only three days from a weak disturbance in the mid-Atlantic Inter-Tropical-Convergence-Zone (ITCZ).

The main focus of this study is on the three storms: ex-Tropical Storm Gaston, pre-Hurricanes Karl and pre-Tropical Storm Matthew. We contrast these data with a brief discussion of those obtained during the mature stage of Hurricane Earl.

In the analyses presented, the negative ocean influence of mixing up of cold water beneath the thermocline to the surface is neglected because the development and non-development of tropical disturbances occurs at relatively low surface winds of approximately 30 knots or less where the impact of wind-induced mixing of cold water is small (Shay, 2010).

3 Dropwindsonde data

Between 20 and 25 dropwindsondes were made during each GV flight mission. Diurnal cycle effects were largely filtered by the fact that the GV flights were carried out at approximately the same time of day. After quality control using the NCAR Aspen software and further manual inspection to eliminate sondes that did not record all the way to the surface, the precise number of usable sondes from the GV is summarized here. For ex-Tropical Storm Gaston: 20 on 2 September, 21 on 3 and 5 September, and 22 on 6 and 7 September. For pre-Hurricane Karl: 21 for the two flights on 10 September and the flights on 11 and 14 September, 22 on 12 September and 20 on 13 September. For pre-Tropical Storm Matthew: 21 on 20, 21 and 24 September and 16 on 22 September. Many of these soundings were released from altitudes between 13 and 14 km giving an unprecedented glimpse of the structure of the much of the tropical troposphere in the systems studied. Radiosonde soundings from island stations at similar latitudes show that the tropopause lies around 15–16 km in the region of interest. Dropwindsonde soundings were made also by the DC8 during the last two days of ex-Tropical Storm Gaston (6–7 September: 6 Sep. 17 usable sondes; 7 Sep. 14 sondes) and for the last three

days of pre-Hurricane Karl (12–14 September: 12 Sep. 18 sondes; 13 Sep. 19 sondes, 14 Sep. 12 sondes).

Because of safety considerations, all of the GV soundings were either in environmental air or on the periphery of convective anvils. Figure 1 shows an example of the distribution of dropsondes in relation to the wave-pouch region of the disturbance pre-Karl on 13 September, and the deep convection and accompanying anvil clouds. The wave-pouch region is identified by the parent wave trough axis (black curve) and the 700 mb streamlines as viewed in the frame of reference moving with the parent wave-like disturbance (the so-called co-moving streamlines). The green curve is the local critical latitude of the parent easterly wave. The intersection between the wave trough and the critical latitude is the so-called ‘sweet spot’, where theory predicts that convection will ultimately organize. Indeed, this location was where the convection did organize on 14 September (see Montgomery *et al.* 2011 for further details). The two figures show the planned flight track and drop points for the GV (top panel) and actual GV flight track (bottom panel) that had to be re-designed in real-time to avoid the line of intense, deep convection oriented in a north-south configuration. Here yellow represents the GV track that is older than two hours and red represents the track that is younger than two hours. The 700 mb co-moving streamlines are shown overlaid with IR images and a lightning and ‘overshooting top’ product from C. Velden’s group on the PREDICT science team (see caption for further details). The inference is that the PREDICT dropsondes were sampling the wave-pouch and its near environment and not clouds *per se*.

The data from all of these soundings were interpolated to levels at intervals of 100 m above the surface. These data were then used to derive various quantities of thermodynamic interest such as the total precipitable water (TPW), Convective Available Potential Energy (CAPE) and Convective Inhibition (CIN). As is well known, CAPE is the *maximum* kinetic energy an ascending air parcel can acquire in ascending to its level of neutral buoyancy (LNB) as a result of the vertical buoyancy force per unit mass. The calculation depends on certain assumptions. Normally, it is assumed that the parcel rises pseudo-adiabatically without mixing with its environment and the latent heat of fusion is neglected. The latter assumption is partly because the precise temperature at which freezing occurs depends on the aerosol content of the parcel, which is not known, although freezing becomes complete at temperatures below -40 C. In this paper we use CAPE as a rough indication of the potential for vigorous updraughts to occur due to buoyancy, but not as a measure of actual convective vigour. Of course, buoyant updraughts cannot be realized unless the CIN is sufficiently small. The method we use for calculating CAPE and CIN is given briefly in the appendix.

The DC-8 sondes were released mostly from altitudes of around 10 km, several kilometres lower than from the GV and often well below the LNB for air parcels lifted from near the surface. For this reason and the fact that CAPE and CIN values turn out to be of limited value

in distinguishing between developing and non-developing systems, CAPE and CIN values were calculated only for the GV sondes.

4 Results

4.1 Ex-Gaston: 2–7 September

Tropical Storm Gaston developed from an African wave and was named by the National Hurricane Center (NHC) at 15 UTC 1 September. However, dropsondes from the GV deployed during its first mission into Gaston on 2 September indicated that the storm had weakened to a tropical depression, whereupon Gaston was officially downgraded to an INVEST⁴. The disturbance maintained an identity that could be tracked across the Caribbean although the convective activity weakened considerably after 7 September. Five GV-flights were made into the disturbance on each day from 2 to 7 September, except on 4 September.

Figure 2 shows objective analyses⁵ of the surface pressure for each of the five flights. The flight tracks, drop points and drop times are shown also. In general, the fields show coherent patterns on a scale larger than the spacing between sondes, a feature that we interpret to be affirmation of the integrity of the data. One surface pressure reading at 1745 UTC on 2 September seemed suspiciously high and was replaced by an average of that from neighbouring points at about the same latitude. Interestingly, the pressure pattern on 2 September has the appearance of a trough, whereas on subsequent days there were some closed isobars (at 0.5 mb spacing), suggesting that Gaston was trying to redevelop. As the main focus of this paper is on the thermodynamical aspects of the systems, the relationship of the surface pressure field to the observed flow field will be discussed in a separate publication.

The right panels in Figure 2 show the corresponding distribution of TPW derived from the sondes. Satellite imagery indicated that Gaston was surrounded by relatively dry air during its westwards transit across the Atlantic and it was speculated by forecasters that this was the reason for Gaston’s failure to redevelop. A Lagrangian perspective on the interaction between the dry environment and the moist pouch will be presented in a separate paper by Rutherford and Montgomery (2011). That work documents the import of dry air into the pouch in the middle troposphere and the severing of the ‘umbilical chord’ of moisture from the ITCZ. For reasons articulated below, these conditions do not favour development.

⁴The term INVEST is used by operational tropical cyclone forecast centres to identify an area of interest for collection of specialized observations or running model guidance. The designation of a system as an INVEST does not correspond to a likelihood of development.

⁵All objective analyses shown in this paper are carried out using a bivariate interpolation method for irregularly spaced points in two dimensions using the subroutine *idbvip* written in Fortran and available from NCAR’s public software library. The method is described in papers by Hiroshi (1978, 1984).

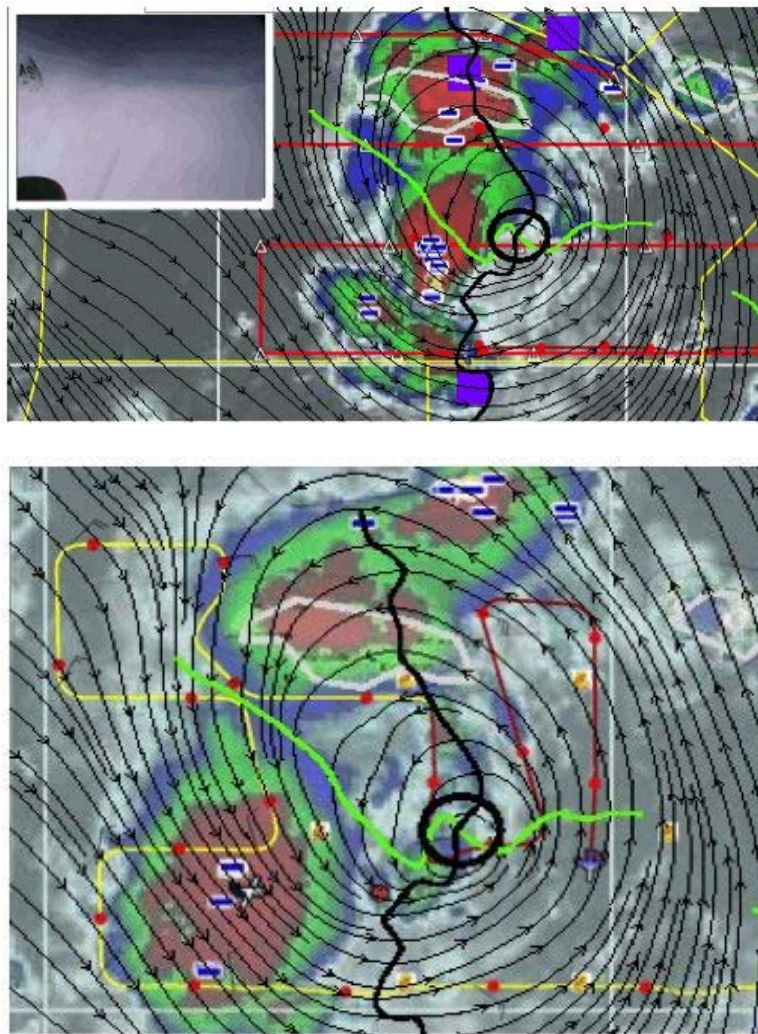


Figure 1. Illustration of forecast tools used by the PREDICT science team of the distribution of dropsondes in relation to the wave-pouch region sampled by the GV aircraft flying between 13 and 14 km altitude. (a) Top panel shows the planned flight path (in red) of the GV within the tropical disturbance ‘pre-Karl’ on 13 September. The chosen time of the satellite image is relatively early in the flight and the aircraft location is indicated by the red aircraft symbol along the bottom flight track. Superimposed on the track is an infrared satellite image at 1137 UTC, indicating the location of deep convection (red denotes cloud tops with temperatures less than -70 Celsius and yellow denotes cloud tops less than -80 Celsius) and accompanying anvil clouds. The regions of active lightning are indicated by the horizontal blue lines and the regions of strong overshooting cloud tops are indicated by the three purple squares. The wave-pouch region is identified by both the (black) wave-trough curve and the ECMWF co-moving streamlines at 12 UTC that re-circulate in a cyclonic sense on the 700 mb surface. The green curve is the local critical latitude of the parent easterly wave where the wave’s zonal phase speed coincides with the local easterly mean flow. The inset on the upper left is a photograph taken from the remote camera onboard the right wing of the GV at the position of the aircraft shown. (b) Zoomed-in view in similar format as (a) with the same co-moving streamline field, but with an updated satellite image at 1426 UTC. Shown is the actual flight path of the GV that was revised during the flight in order to avoid penetrating the region of vigorous deep convection (yellow color) that was emerging directly ahead of the GV’s track. The second aircraft symbol in this image (lower left) denotes the location of the NOAA P-3 aircraft that was flying a coordinated mission with the GV in order to sample the convective region with the airborne Doppler radar system at lower altitude of approximately 4 km altitude. Other features are as described in (a). For further details see text and PREDICT science summaries available at: <http://catalog.eol.ucar.edu/cgi-bin/predict/report/index>.

The presence of dry air is confirmed by the TPW-analyses and especially on 5 September, dry air is seen to be wrapping around the southern side of the depression. Nevertheless the core, or pouch region, maintains relatively high TPW values ($> 50 \text{ kg m}^{-2}$) throughout the period of study. Indeed, we present evidence below to show that the lower troposphere actually moistened during the five aircraft missions, although the middle and upper troposphere did not (see Figure 8). It will be noted that the highest TPW values lie broadly within the region of

lowest surface pressures on all days and encompass the sweet spot. Figure 3 shows frequency diagrams of TPW-values from the five flights. Significantly, the percentage of *relatively high* TPW-values ($\geq 55 \text{ kg m}^{-2}$) on the five days and the number of usable sondes (in brackets) were 55% (20), 67% (21), 48% (21), 33% (22) and 45% (22), respectively. It is interesting to compare these percentages with the corresponding ones for pre-Hurricane Karl given in section 4.2, which are considerably higher.

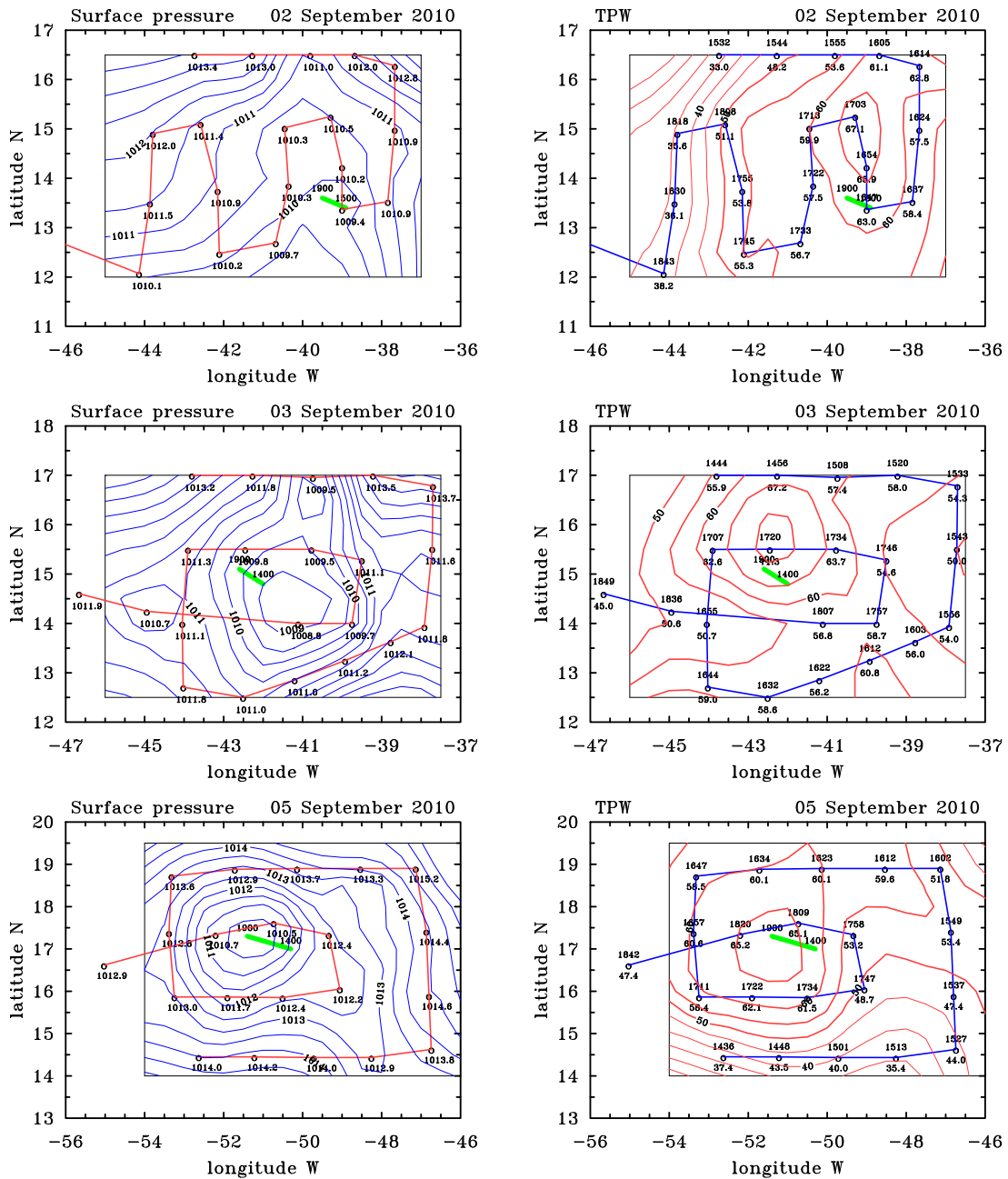


Figure 2. Objective analyses of surface pressure (left panels) and total precipitable water (right panels) for ex-Tropical Storm Gaston on 02, 03 and 05 September 2010. Contour interval 0.5 mb for pressure, 5 kg m⁻² for TPW. The aircraft track is marked with the location of soundings along the track (small circles). The data are given below the circle and time of the sounding in UTC is given above the circle in the TPW plots. The original surface pressure from the sounding at 1745 UTC on 2 September was suspiciously high (1015.6 mb) and was replaced by the average of the two adjacent values at 1733 UTC and 1843 UTC. The approximate track of the pouch centre during the flight with starting and ending times indicated is marked by the thick (green) line. Figure continued on the next page.

Figure 4 shows the vertical structure of virtual potential temperature (θ_v), pseudo-equivalent potential temperature⁶ (θ_e), and saturation pseudo-equivalent potential temperature (θ_{es}) for four selected soundings on 5 September, two in the region of highest TPW and two in the dry air to the south of this region. The vertical lines in the figure show the θ_e values for air parcels at the surface and at a height of 100 m above the surface. Since θ_e is

⁶The pseudo-equivalent potential temperature was calculated using Bolton's formula (Bolton 1980).

conserved for undilute ascent with or without condensation, these lines represent the θ_e of moist air parcels lifted from these levels. Moreover, the distance between the vertical line and the θ_{es} -curve at a given height is roughly proportional to the buoyancy of the lifted air parcel at this height, with the buoyancy being positive when the parcel line is to the right of the θ_{es} -curve. Thus, assuming undilute ascent, the first intersection of the vertical line with the θ_{es} -curve is the approximate level of free convection (LFC) and the final intersection is approximately equal to the LNB for the particular air parcel (see Ooyama

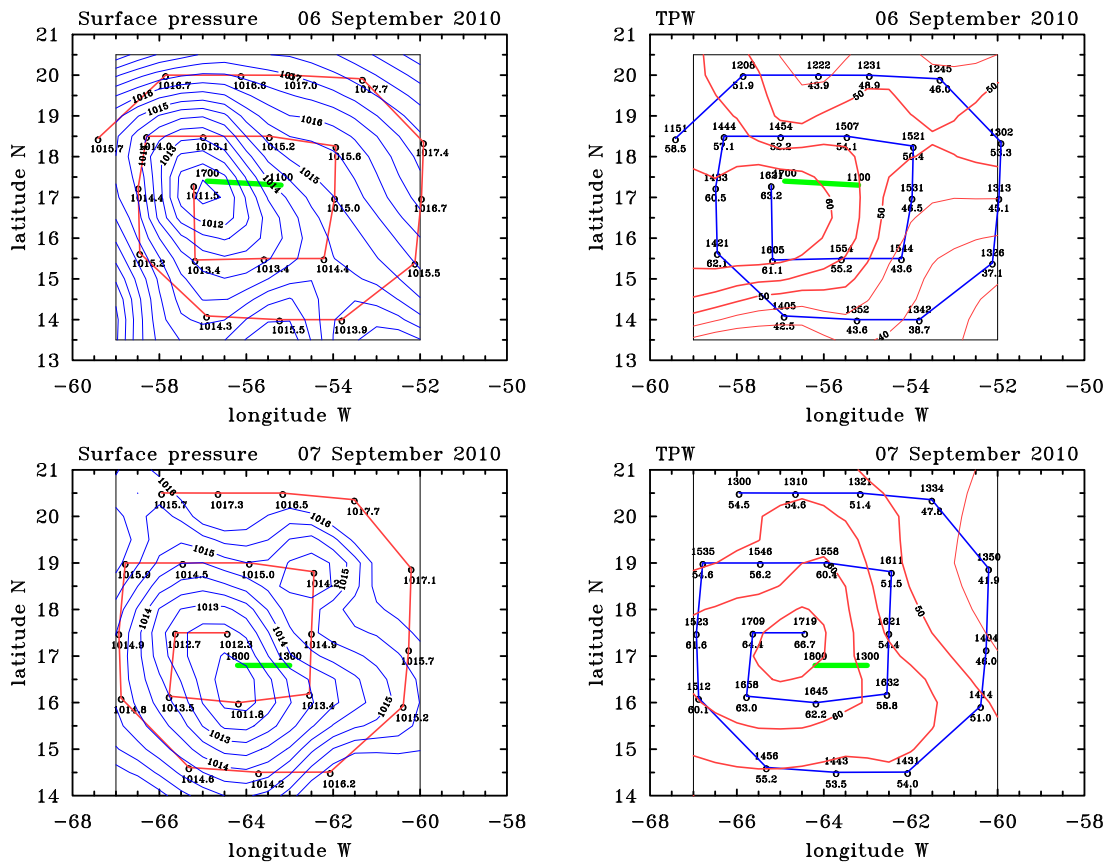


Figure 2. (continued) Objective analyses of surface pressure (left panels) and total precipitable water (TPW) (right panels) for ex-Tropical Storm Gaston on 06 and 07 September 2010. Contour interval 0.5 mb for pressure, 5 kg m^{-2} for TPW.

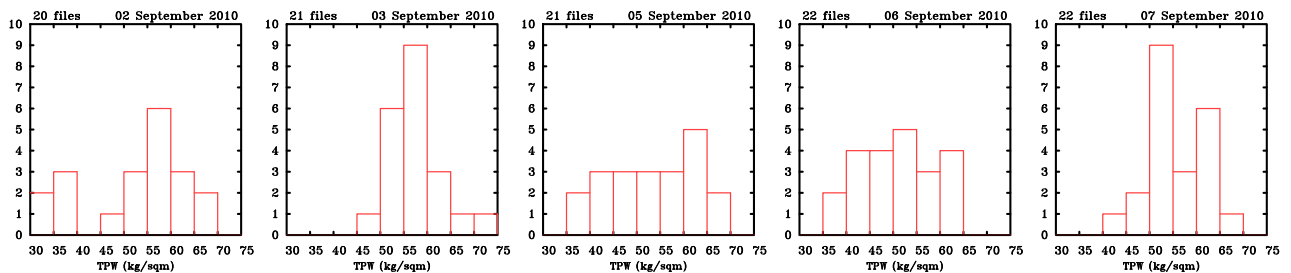


Figure 3. Frequency diagrams of TPW for ex-Gaston on 02, 03, 05, 06 and 07 September 2010.

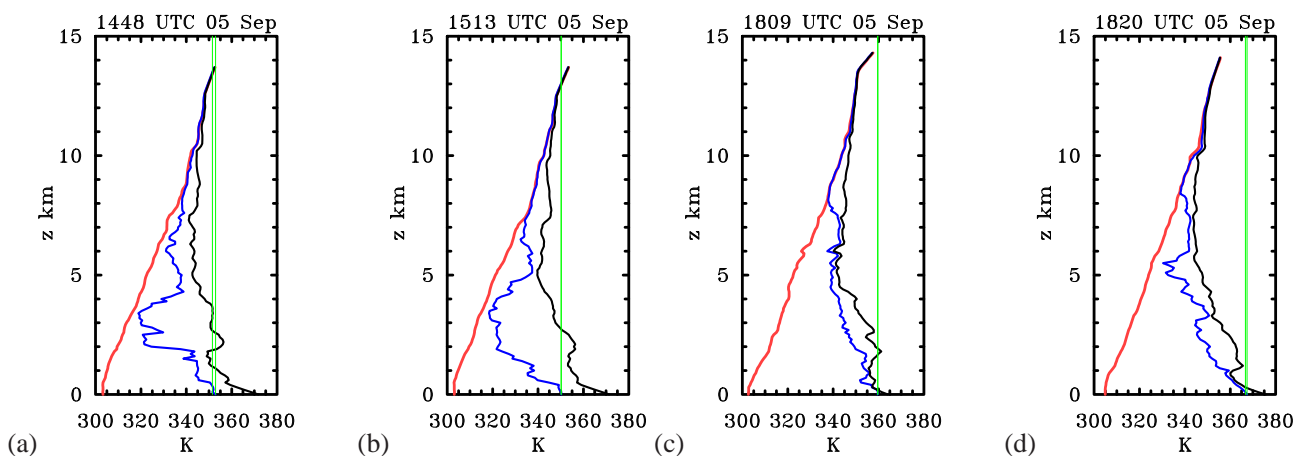


Figure 4. Four soundings for ex-Gaston on 05 September: (a) 1448 UTC; (b) 1513 UTC; (c) 1809 UTC; (d) 1820 UTC. See Fig. 2 for positions in relation to TPW. The left (red) curves show θ_v , the middle (blue) curves show θ_e , and the right (black curves) θ_{es} . The vertical lines show values of θ_e for air parcels at the surface and 100 m. The intersection of these lines with the θ_{es} show the approximate locations of the LFC and LNB. See text for discussion.

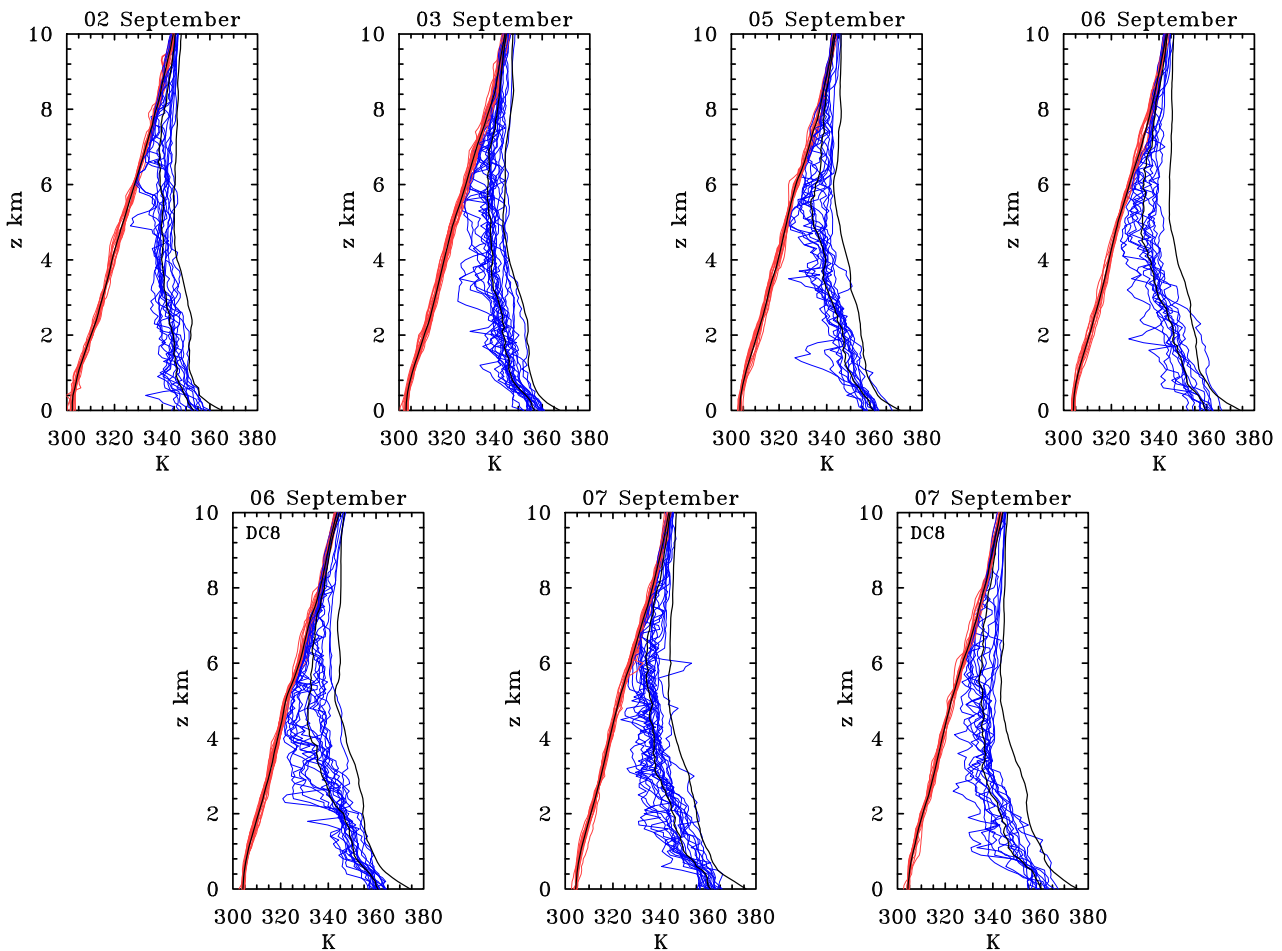


Figure 5. All soundings of θ_v (red curves) and θ_e (blue curves) for Gaston on 02, 03 and 05–07 September 2010 as indicated. The pouch-means of θ_v , θ_e are indicated by black curves. The right black curve is the θ_{es} for the pouch-mean sounding. The left and right panels show soundings from the NASA DC-8 flights on 6 and 7 September.

1969, Emanuel 1994, Holton 2004). Furthermore, the area between these lines and the θ_{es} -curve in the range between the LFC and LNB is roughly proportional to the CAPE and that between the surface and the LFC is roughly proportional to the CIN. The following features may be noted:

- The height from which the soundings were made was mostly close to the LNB allowing reasonably accurate estimates of CAPE⁷.
- The vertical structure of θ_v shows the expected monotonic increase with height and varies little between soundings.
- The LFC of the two soundings on the southern side of the domain is relatively high and, judged directly from these figures, these soundings have considerably lower CAPE than the two moist soundings⁸. Indeed, air parcels lifted from, or near, the surface acquire little or no buoyancy below a height of about 4 km. A striking feature of these sounding is the low values of θ_e in the low to middle troposphere,

there being a large saturation deficit, as measured by $\theta_{es} - \theta_e$, exceeding 30 K. (Here θ_{es} is the saturation value of θ_e .) These values indicate the presence of relatively dry air at these levels.

- The LFC of the two moist soundings is much lower than the two dry ones and the CIN is correspondingly lower. Moreover, the buoyancy of lifted air parcels is much larger, whereupon the values of CAPE are much larger also. For these soundings, the saturation deficit is relatively small throughout much of the troposphere.

Figure 5 shows similar profiles of all soundings with a TPW equal to or higher than 50 kg m^{-2} together with their mean on each day of measurement⁹. The foregoing criterion was found to correspond roughly with the region of closed streamline contours at 700 mb in the European Centre for Medium Range Weather Forecasts (ECMWF) analysis near the time of the mission and eliminated only a small fraction of soundings on the periphery of the system.

⁷In cases where the LNB was above the sounding, the sounding was extended, guided by that in the European Centre for Medium Range Weather Forecasts analyses in the storm location.

⁸Actual values of CAPE, calculated by the method given in an appendix, are shown in Figure 6.

⁹The number and percentage (in brackets) of soundings with TPW > 50 kg m^{-2} was 14 (70%), 20 (90%), 14 (67%), 12 (55%), 19 (86%) on 2, 3, 5, 6, 7 September, respectively

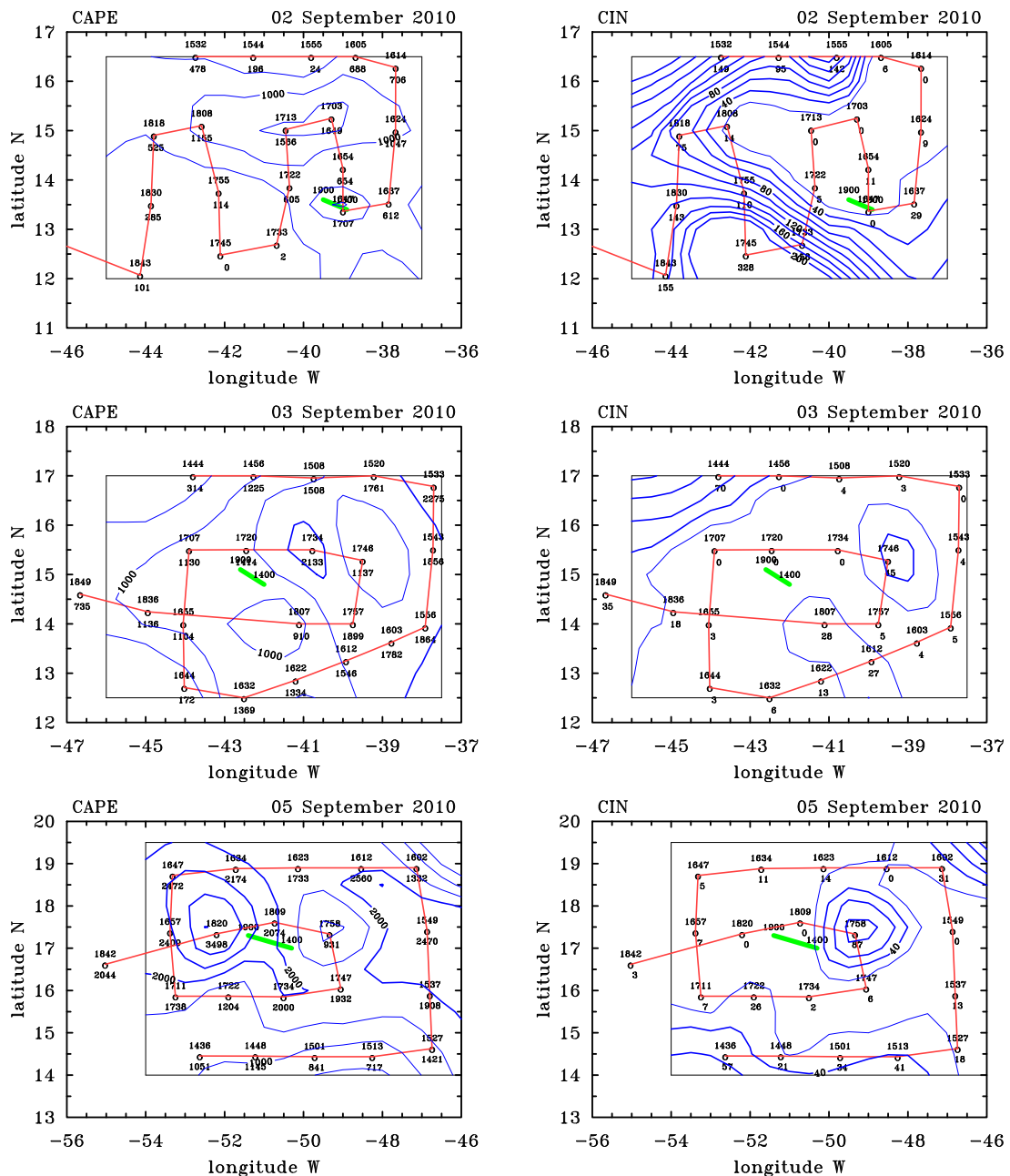


Figure 6. Objective analyses of CAPE (left panels) and CIN (right panels) for ex-TS Gaston on 02, 03 and 05 September 2010. Contour interval for CAPE: 500 J kg^{-1} , values 2000 J kg^{-1} or more in bold. Contour interval for CIN: 20 J kg^{-1} , values 40 J kg^{-1} or more in bold. The aircraft track is marked with the location of soundings along the track (small circles). The time of the sounding in UTC is given above the circle and the data below the circle. The approximate track of the pouch centre during the flight with starting and ending times indicated is marked by the thick (green) line. Figure continued on the next page.

Therefore, this value of TPW is used throughout this study as a rough proxy for the pouch.

Consistent with the four soundings shown in Figure 4, the vertical structure of θ_v shows little variability between soundings. However, there is considerable variability in the vertical structure of θ_e on a particular day. The variability between the daily-mean soundings is discussed later (see Figure 8). On all days, the vast majority of the θ_e curves lie to the left of the θ_{es} -curve for the mean sounding.

Figure 6 shows the spatial distribution of CAPE and CIN for the five missions into ex-Gaston and Figure 7

shows a scatter plot of CAPE and CIN for all soundings, identified by day. Figure 6 shows also the track segment of the sweet spot during the flight mission. The following features are evident:

- On all days there are some relatively high values of CAPE ($> 1500 \text{ J kg}^{-1}$), with the maximum values increasing from day to day. On the last three missions, between one and five soundings have values exceeding 3000 J kg^{-1} , the most being on 7 September.

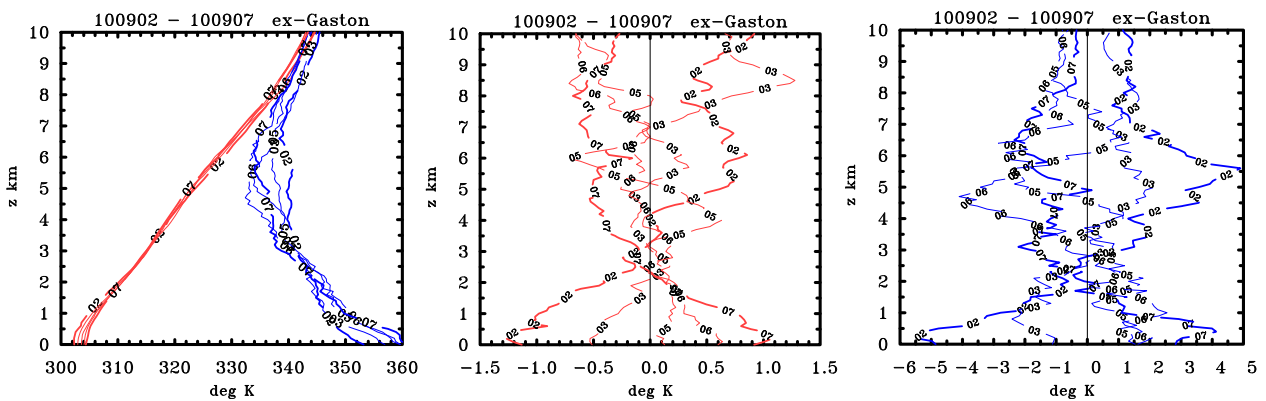


Figure 8. Vertical profiles of θ_v and θ_e (left panels); vertical profiles of daily departures of θ_v (middle panel) and θ_e (right panels) from mean profiles for all days for ex-Tropical Storm Gaston on 02, 03, 05, 06, 07 September, 2010. The thick curves mark the first and last days of the GV flights. Numbers on curves refer to the date. Curves for the NASA DC-8 flights on 06 and 07 September are denoted D6 and D7 respectively.

“pouch-mean” soundings obtained from the dropsondes during missions into ex-Gaston. These pouch-mean soundings are characterized by the virtual potential temperature (θ_v) and pseudo-equivalent potential temperature (θ_e) as a function of height. The middle and right panels of Figure 8 show the deviations of θ_v and θ_e from the five day mean. Features that stand out are as follows:

- There is little difference in the day-to-day variation in the system-average θ_v .
- There is a general day-to-day increase in the lower tropospheric θ_e , but at mid-upper levels ($z > 3$ km), the mean θ_e decreases with time.
- There is a monotonic warming of the lowest 2 km, exceeding 2 K near the surface. Above 3 km altitude, there is cooling on the order of 1 to 1.5 K at all heights up to at least 10 km.
- There is a relatively large difference (typically 25 K) between near-surface θ_e value and those of the mid-troposphere minimum.

It is reasonable to speculate that the warming and at least part of the increase in θ_e at low levels is due to the increase in sea-surface temperature (about 1° C) as ex-Gaston moved across the Atlantic Ocean and then over the warmer Caribbean Sea.

Traditional reasoning would suggest that ensuing convection within a relatively dry mid-upper air environment would lead to comparatively-strong downdraughts (e.g. Emanuel 1994). From the perspective of convective dynamics, stronger downdraughts (implied by the lower mid-tropospheric relative humidity in Gaston) would tend to import low θ_e into the boundary layer and frustrate the enhancement of boundary layer θ_e by sea-to-air moisture fluxes. This enhancement is necessary to fuel subsequent deep convective activity. However, recent numerical modelling studies by James and Markowski (2009) and Kilroy and Smith (2011) suggest that the principal effects of the dry air are to reduce the updraught strength and water loading, while the downdraught strengths are not changed appreciably. The dilution of the updraught with dry air

would reduce cloud buoyancy making the updraught less effective in amplifying vertical vorticity throughout a significant depth (see section 5).

As to the source of this drier air in ex-Gaston, there is evidence of a strong, dry Saharan air mass surrounding the northern hemisphere of ex-Gaston in multiple satellite derived products. A Lagrangian analysis carried out by Rutherford and Montgomery (2011) indicates strongly that the dry air seen in the observations is the result of a complex process of intrusion of dry air from outside of the pouch region. Dry air continued to plague ex-Gaston during the subsequent days. The cyclonic circulation became shallower over time also (Davis, personal communication, Boothe, personal communication). By 5 September, the circulation was not evident at 500 mb and by 7 September it was barely evident at 700 mb. The storm continued to produce intense convection intermittently throughout the period, but the vortex systematically weakened.

4.2 Pre-Hurricane Karl: 10-14 September

The disturbance that ultimately became Hurricane Karl originated within the Inter-Tropical Convergence Zone (ITCZ) region near the northern coast of South America. A surge of southwesterlies over northern South America around 8 September was accompanied by the formation of a quasi-persistent area of convection along the ITCZ near the northern coast of the Continent. An easterly wave formed subsequently near this locale and propagated westwards towards the eastern Caribbean. Convection within the early pre-Karl disturbance was elongated east-west on 10 September. On this day, two missions were conducted, one centred on roughly 13 UTC, the other about 6 h later. Both flights revealed a broad cyclonic wind gyre of diameter roughly 400 km that featured similar tangential winds between 950 mb and 700 mb (Boothe, personal communication). Pre-Karl was rather slow to develop over the next several days. Over the course of 11-14 September, convective activity gradually consolidated from an initial southwest-northeast elongation to a more

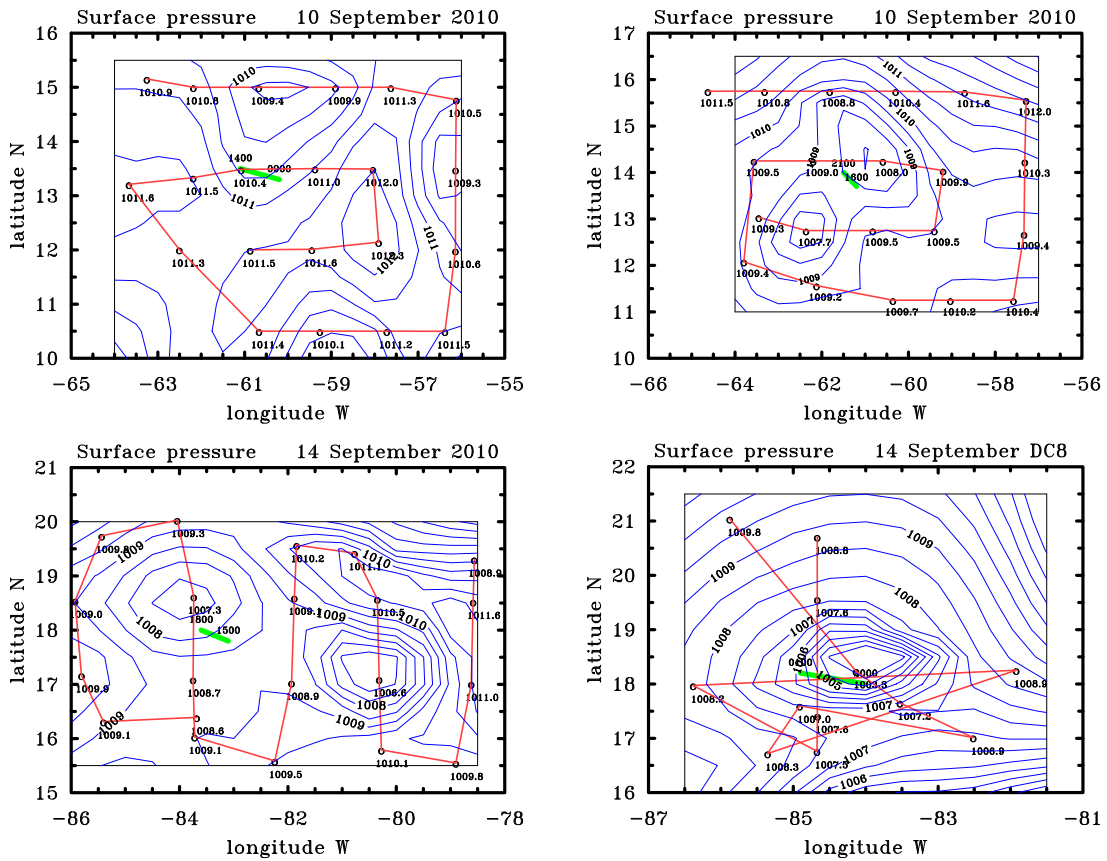


Figure 9. Objective analyses of surface pressure for the two GV flights into pre-Hurricane Karl on the first day of observations (10 September) and the two flights on the last day (14 September), the last one being the DC-8 flight. Contour interval 0.5 mb for pressure. The aircraft track is marked with the location of soundings along the track (small circles) and the data are given below the circle. The approximate track of the pouch centre during the flight with starting and ending times indicated is marked by the thick (green) line.

compact pattern encircling the sweet spot within the pouch, the latter being close to the location where Karl formed later on 14 September.

Figure 9 shows objective analyses of the surface pressure for the first two flights, on 10 September, and the last two on 14 September. As in Figure 2, the flight tracks, drop points and drop times are shown also, together with the track of the sweet spot during the flight. On 12 September, the flight tracks as well as the location and timing of dropsondes were unsuitable for objective analysis. As in the case of ex-Gaston, the analyses show coherent patterns on a scale larger than the spacing between sondes. However, unlike ex-Gaston, the pressure patterns from the analyses show multiple centres with closed isobars as late as the first GV mission on 14 September, approximately 6 hours prior to the disturbance being declared a tropical storm. Although the later flight by the NASA DC-8 found a single pressure minimum at the surface (cf. Figure 9d), we caution that this minimum is based on only one sounding.

Only three soundings (all on 13 September) had values of TPW less than 50 kg m^{-2} , while 50% of soundings had values exceeding 60 kg m^{-2} , compared with only 26% for Gaston. For this reason, plots of TPW are not shown for Karl. However, we note that, as in

Gaston, the highest TPW values lay broadly within the region of lowest surface pressures on all days.

Figure 10 shows the spatial distribution of CAPE and CIN for the two flights on 10 September and the flights on 11, 13 and 14 September. The corresponding scatter plot for these data analogous to that shown for ex-Gaston (Figure 7) are shown in Figure 11. Like ex-Gaston, on all days there are some relatively high values of CAPE. The higher values of CAPE have relatively low values of CIN. However, unlike ex-Gaston, there are no values of CAPE exceeding 3000 J kg^{-1} . There was a slight increase in the percentage of sondes having CAPE values larger than certain thresholds (see below). Furthermore, the highest values of CAPE are not near the sweet spot position.

Some statistics can be derived also from these data using frequency diagrams (not shown):

- Discounting the CAPE values from the second flight on 10 September, which was made at a different time of day from the others, between 57% and 71% of soundings over the GV missions had values of CAPE exceeding 1500 J kg^{-1} and between 14% and 19% of soundings on the last three days have values exceeding 2500 J kg^{-1} , the largest percentages being on 14 September.

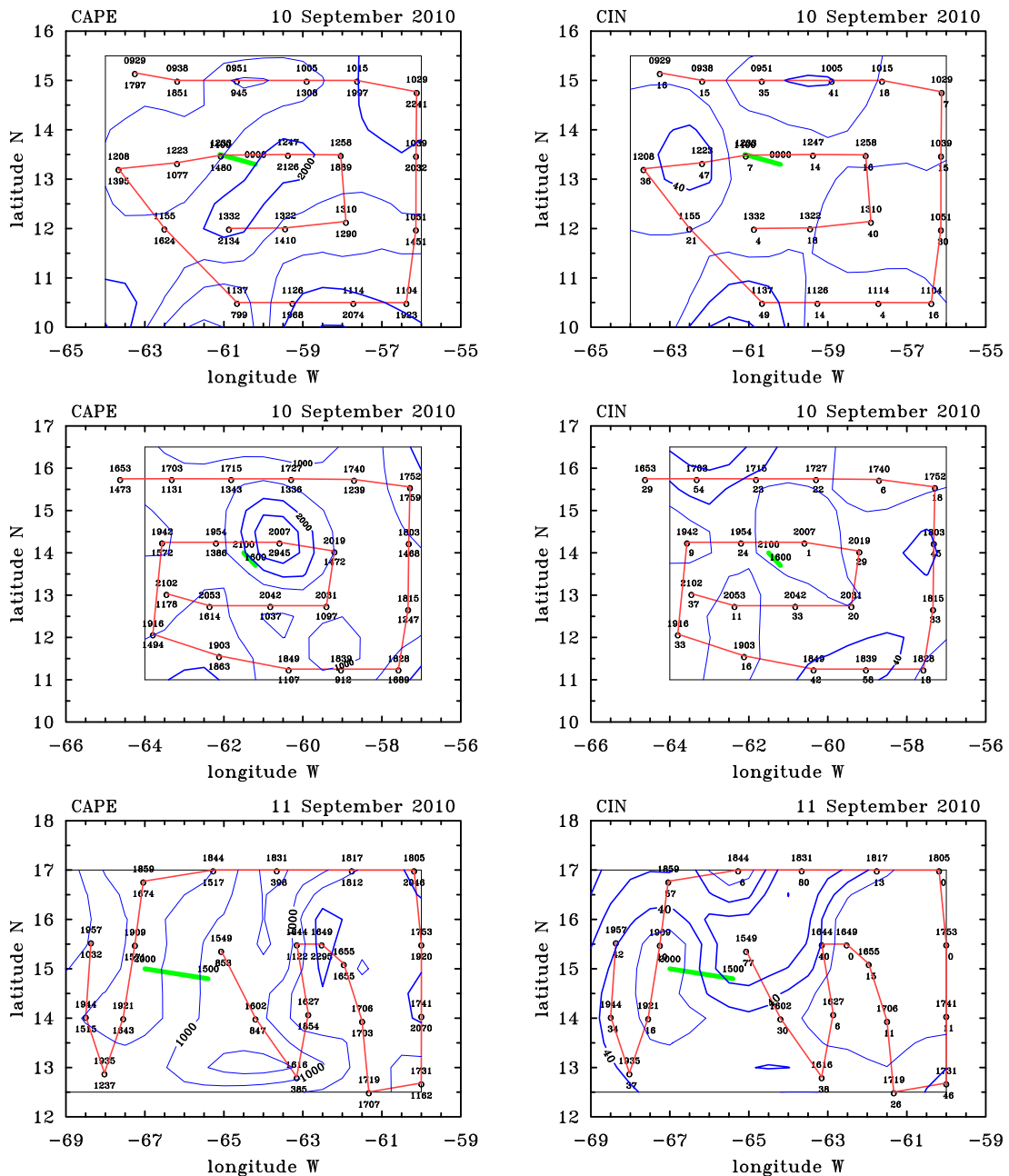


Figure 10. Objective analyses of CAPE (left columns) and CIN (right columns) for pre-Hurricane Karl on 10 and 11 September 2010. There were two flights on 10 September. Contour interval for CAPE: 500 J kg^{-1} , values 2000 J kg^{-1} or more in bold. Contour interval for CIN: 20 J kg^{-1} , values 40 J kg^{-1} or more in bold. The aircraft track is marked with the location of soundings along the track (small circles). The time of the sounding in UTC is given above the circle and the data below the circle. The approximate track of the pouch centre during the flight with starting and ending times indicated is marked by the thick (green) line. Figure continued on the next page.

- Between 71% and 85% of soundings have values of CIN below 40 J kg^{-1} and between 33% and 80% have values below 20 J kg^{-1} , the largest percentages of the latter being on 13 September (80%) and 14 September 76%.

Figure 12 shows profiles of all soundings with a TPW $\geq 50 \text{ kg m}^{-2}$ together with their mean on each day of measurement in pre-Karl. As in the case of ex-Gaston, the soundings are characterized by the vertical profiles of θ_v and θ_e . The main points to note are that there is little variation between soundings for θ_v and the scatter in θ_e is

significantly less than that in Figure 4. In addition, the vast majority of the θ_e curves lie to the left of the θ_{es} curves for the mean sounding.

The left panel of Figure 13 shows the day-to-day evolution of the pouch-mean soundings obtained from the dropsondes. The middle and right panels show the deviations of θ_v and θ_e from the five day mean. Features that stand out are:

- As for ex-Gaston, there is little difference in the day-to-day variation in the system-average θ_v .

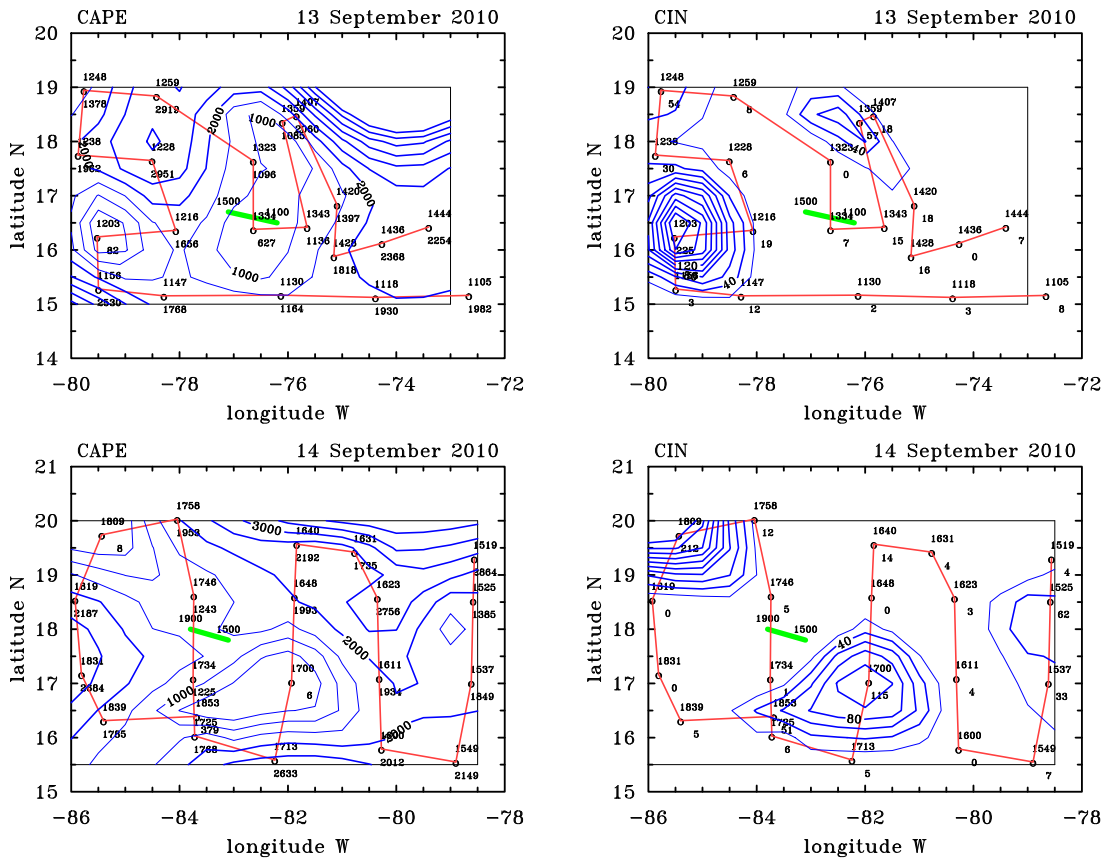


Figure 10. (continued) Objective analyses of CAPE (left columns) and CIN (right columns) for pre-Hurricane Karl on 13 and 14 September 2010.

- There is a general day-to-day increase in the lower tropospheric θ_e . However, unlike the case of ex-Gaston, the mean θ_e at mid-upper levels ($z > 3\text{km}$) increases over the period of observation, but this increase is not monotonic.
- There is a systematic warming of the entire troposphere between 10 and 14 September. Between the surface and 5 km altitude the warming is on the order of 0.7 K. Above 5 km, the warming increases with height and exceeds 3 K above about 9 km altitude.
- There is only a modest difference ($\sim 15\text{ K}$) between the near-surface θ_e and the mid-tropospheric minimum. This is in contrast to the $\sim 25\text{ K}$ difference in the non-developing ex-Gaston.

4.3 Pre-Matthew: 20-24 September

In contrast with Karl, Matthew was generally unforeseen as few as 5 days prior to its formation. While the PREDICT team was tracking weak vorticity features connected with the ITCZ on 17 and 18 September, it was not until deep convection erupted on 19 September that there was a feature sufficiently defined in the atmosphere and in global models to plan a mission. The first GV mission was centred roughly on 16 UTC 20 September. At this time, the pre-Matthew disturbance appeared less organized than Karl when it was first flown. However, Matthew quickly organized on 21 and 22 September.

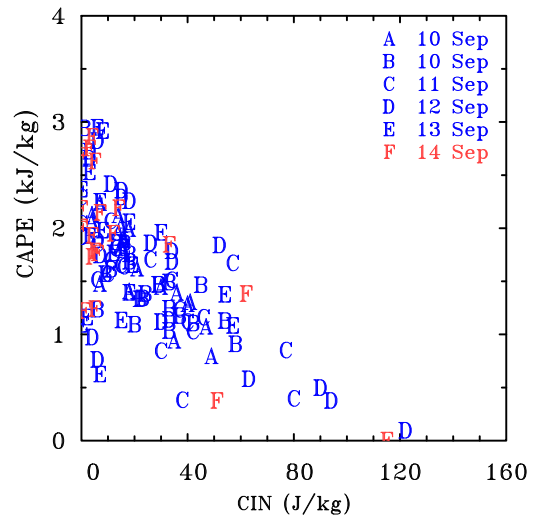


Figure 11. Scatter plots of CAPE and CIN values for the 106 soundings in pre-Karl. Note the tendency for soundings with high values of CAPE to have low values of CIN.

The pouch was well defined on 22 September with strong convection occurring close to the predicted maximum in Okubo-Weiss parameter in the analysis from the ECMWF model (see Montgomery *et al.* for details). Matthew went on to develop into a strong tropical storm on 23 September, but despite forecasts of potential rapid

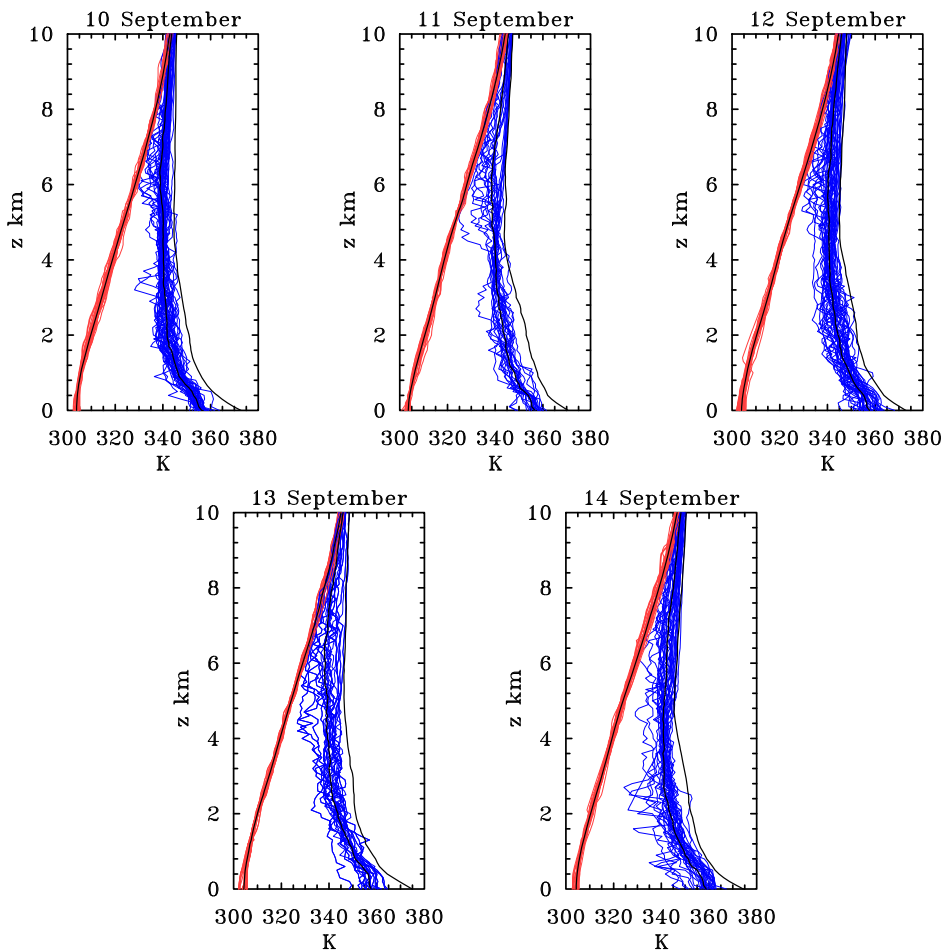


Figure 12. All pouch soundings of θ_v (red curves) and θ_e (blue curves) for pre-Karl on 10–14 September 2010 as indicated. The pouch-means of θ_v , θ_e are indicated by black curves. The right black curve is the $\theta_{e,s}$ for the pouch-mean sounding. The upper left panel (a) contains data for both flights on 10 September, while the upper right and two lower panels include both the GV and NASA DC-8 data.

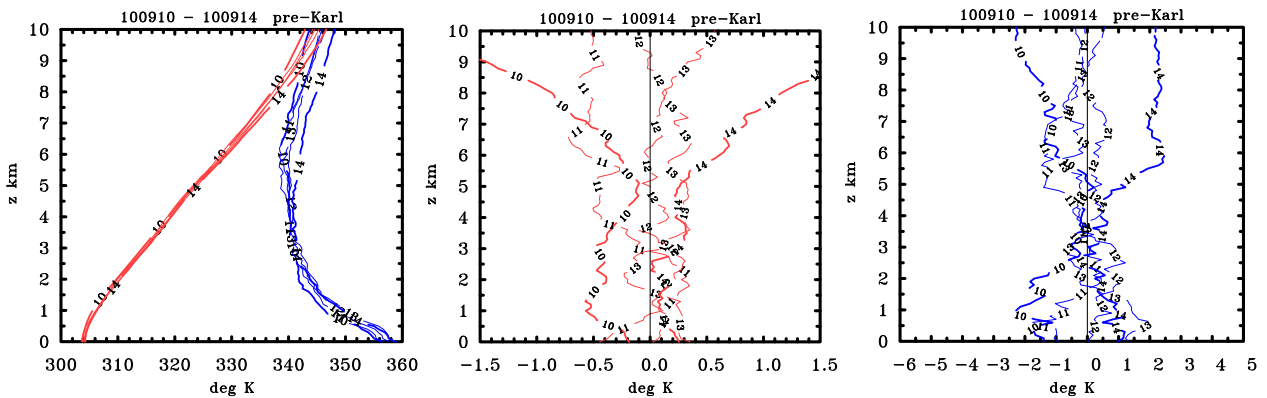


Figure 13. Vertical profiles of θ_v and θ_e (left panels); vertical profiles of daily departures of θ_v (middle panel) and θ_e (right panels) from mean profiles for all days for pre-Hurricane Karl on 10–14 September, 2010. The thick curves mark the first and last days of the sequence. Numbers on curves refer to the date. The profiles on 10 September include both GV flights and those for 12–14 September include both GV and DC-8 data.

intensification, it did not intensify further and made land-fall in Belize as a moderate tropical storm late on 24 September. Although it had similarities to Karl in its mid-ocean origin and track through the Caribbean, Matthew developed rapidly, but failed to become a hurricane.

Figure 14 shows a scatter plot of CAPE against CIN for the GV soundings obtained in Matthew. Unlike the

case of pre-Karl and ex-Gaston, CAPE values are generally largest on the first day of observation (20 September) with 52% soundings having CAPE exceeding 1500 J kg^{-1} : this percentage declined to 19% on 21 September and only 14% on 24 September. There is only one value of CAPE exceeding 2500 J kg^{-1} and that occurs on 20 September. The highest percentages of CIN values

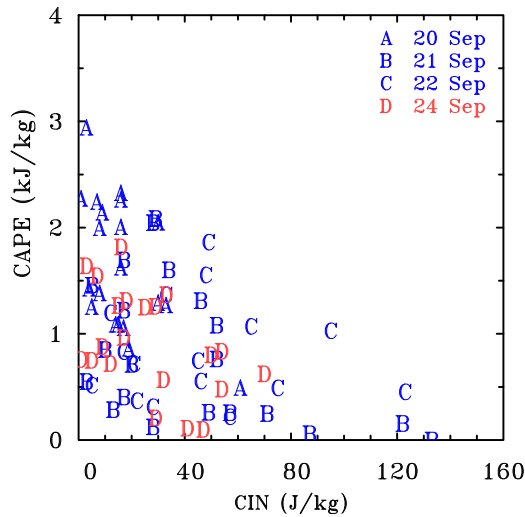


Figure 14. Scatter plot of CAPE and CIN values for the 79 soundings in pre-Matthew.

less than 20 J kg^{-1} and less than 40 J kg^{-1} are on 20 September (76% and 90%, respectively). These percentages decline monotonically over the next two days to 19% and 44%, respectively, and then resurge on 24 September to 48% and 71%, by which time the disturbance had been declared a tropical storm. As in the case of ex-Gaston and pre-Karl, the evolution of CAPE and CIN do not appear to provide clues to possibility of development or non-development.

The left panel of Figure 15 shows the day-to-day evolution of the pouch-mean soundings obtained from the dropsondes. The middle and right panels show the deviations of θ_v and θ_e from the four day mean. Features that stand out are:

- As for ex-Gaston and pre-Karl, there is little difference in the day-to-day variation in the system-average θ_v .
- Unlike ex-Gaston and pre-Karl, there is an overall increase in the lower tropospheric θ_e over the four days of observation, but the θ_e initially decreases and then increases. There is little difference in the mean θ_e over the first three days at mid-upper levels ($z > 3 \text{ km}$), but over the next two days the θ_e increases by approximately 2 K. Initially, there is only a modest difference ($\sim 15 \text{ K}$) between the near-surface θ_e and the mid-tropospheric minimum. This difference is similar to that found in Karl.
- Between 20 and 21 September there is a slight cooling in the virtual potential temperature below an altitude of 6 km of approximately 1 K. On subsequent days there is a systematic warming on the order of 1.5 K.
- Like the virtual potential temperature, the deviation of θ_e from the five day mean falls about 4 K below 2 km altitude. Above this altitude, there is no appreciable change up to 22 September, after which there is a systematic increase of approximately 2 K.

4.4 Hurricane Earl: 1-2 September

Figure 16 shows the profiles of all soundings together with their mean on two days of measurement during NASA DC-8 missions into Hurricane Earl. There were 25 soundings on 1 September and 29 soundings on 2 September. Although the mature hurricane was not a theme of the PREDICT experiment, it is of interest to contrast the soundings in a fully-fledged hurricane with those observed in the pre-storm stage of evolution. Both the θ_v and θ_e curves show much more variability than found in ex-Gaston and pre-Karl (compare Figure 16 with Figures 5 and 12). A distinct feature of these profiles is the set of "eye" and "eyewall" wall soundings, which have significantly higher values of θ_e than were recorded in any of the pre-storms. These soundings are distinctly warmer in terms of virtual potential temperature than those outside of the eye-eyewall region. Note that the eye and eyewall profiles of θ_e are almost vertical and lie well to the right (by approximately 10 K) of the mean saturation θ_e of the averaged temperature of all soundings. This feature is indicative of moist adiabatic ascent up to flight level.

5 Discussion and Interpretation

Over the years, the life cycle of individual deep convective clouds has been well documented and there have been text books written on the subject (e.g. Emanuel 1994, Cotton and Anthes 1994, Houze 1994). It is known that such clouds have a lifetime of an hour or less. During their developing phase they remove moist air from the lowest 1-2 km and carry it into the upper troposphere. As their updraughts become loaded with liquid water and/or ice, the lower part of the updraught decays and becomes a downdraught. The downdraught is driven by the collective drag of precipitation and, below cloud base, also to the cooling of air resulting from evaporation of the precipitation as it falls through unsaturated air. The collective effect of downdraughts is to spread a thin carpet of cool air near the surface that tends to stabilize the air to subsequent convection. Mixing and detrainment from a spectrum of convective cells with air in the cloud environment leads to a moistening of the environment in middle and upper levels.

The traditional argument has been that downdraughts tend to be stronger when the middle-layer air in the cloud environment is dry, but this view has been challenged recently. In section 4.1, it was argued that the failure of Gaston to re-develop was traceable to the injection of dry air into Gaston's pouch near the middle levels. If the foregoing mechanisms are operating, the implications of this dry air would be a cooling and drying of the near-surface air. However, precisely the opposite is observed! In particular, the boundary layer θ_e increased progressively over the entire observation period and yet the system did not develop. While there may be several potential explanations for this behaviour, these findings raise a basic question. What are the consequences of the dry air on the ability of the clouds to amplify the background rotation?

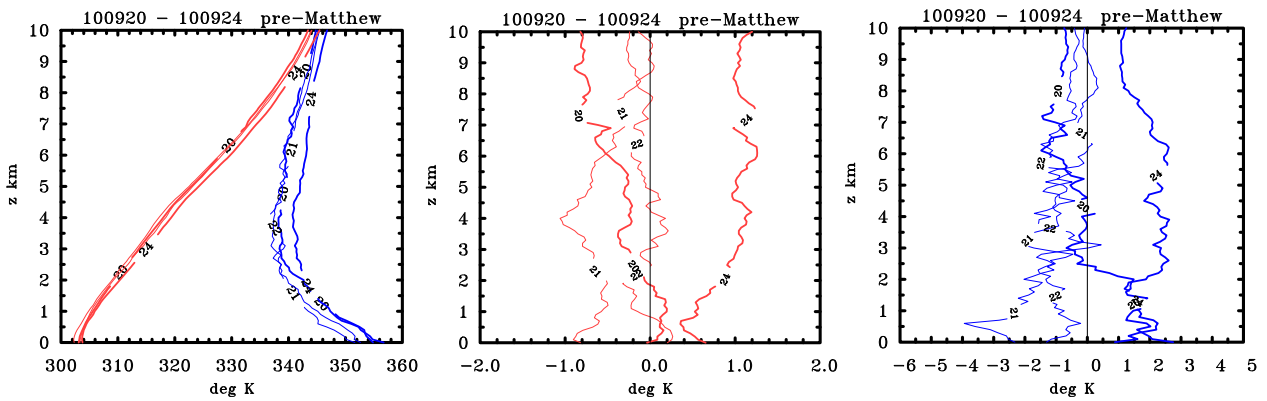


Figure 15. Vertical profiles of θ_v and θ_e (left panels); vertical profiles of daily departures of θ_v (middle panel) and θ_e (right panels) from mean profiles for pre-Matthew on 20-22 and 24 September. The thick curves mark the first and last days of the sequence. Numbers on curves refer to the date.

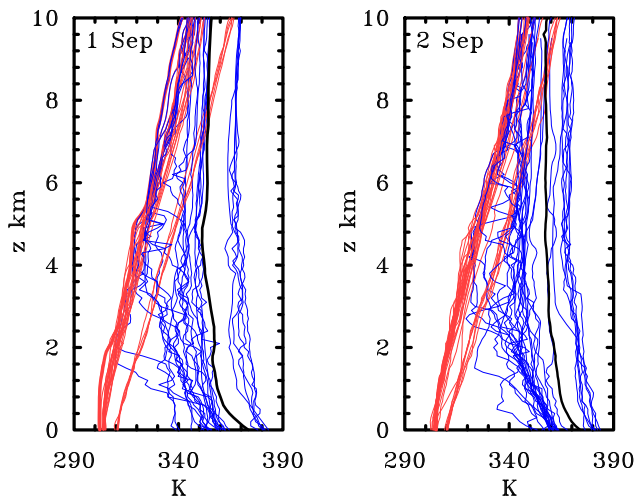


Figure 16. All soundings of θ_v (red curves) and θ_e (blue curves) for Hurricane Earl on 01-02 September 2010 as indicated. The black line is the saturation θ_e of the mean sounding.

When convection occurs in an environment of non-zero vertical vorticity, basic fluid dynamical considerations suggest that updraughts would amplify the vorticity by the process of vortex-tube stretching. Even for background rotation rates as low as that of an undisturbed tropical atmosphere away from the equator, cloud model simulations confirm this tendency to amplify planetary vorticity on time scales of an hour (Saunders and Montgomery, 2004; Wissmeier and Smith 2011). A striking result of such simulations is the exceedingly large amplification of the vertical component of relative vorticity, which is a maximum at low levels and which persists long after the initial updraught has decayed. These cloud model simulations indicate also that the induced tangential wind speeds by a single updraught is typically no more than a few meters per second with a horizontal scale of around 10 km, and would be barely detectable by normal measurement methods in the presence of an ambient wind field. Together these results suggest that all non-shallow tropical convection away from the equator is vortical to some degree and can amplify the vertical vorticity locally by

between one and two orders of magnitude. It is not hard to imagine, then, that the stretching of vertical vortex tubes by a developing cumulus cloud is a fundamental process and that it may be an important process in tropical cyclogenesis.

These vortical convective clouds have been identified as fundamental building blocks during both the tropical cyclone genesis and intensification process (Hendricks *et al.* 2004, Montgomery *et al.* 2006, Braun *et al.* 2010, Fang and Zhang, 2010, Nguyen *et al.* 2008, Montgomery and Smith 2011). The vertical vorticity that is generated by the clouds outlives the convection that produced them in the first place. The like-signed vortical remnants tend to aggregate in a quasi two-dimensional manner with a corresponding upscale energy cascade and some of these remnants will be intensified further by subsequent convective episodes. If the disturbance-scale circulation strengthens, they will tend to become axisymmetrized by the associated angular shear flow. In addition, system-scale inflow forced by the aggregate latent heating from the convective elements leads to an inward advection of convectively-enhanced vorticity. Stokes' theorem applied to a fixed area *surrounding the convection* implies that there will be an accompanying increase in strength of the disturbance-scale circulation on account of the import¹⁰ of ambient absolute vorticity into it. When applied to a fixed area *within the convective region*, the import of convectively-enhanced vorticity into the area will lead also to an increase in the circulation. As the circulation progressively increases in strength, there is some increase in the surface moisture fluxes. However, it is not necessary that the moisture fluxes continue to increase with surface wind speed (Montgomery *et al.* 2009). This research forms the basis of a unified view of tropical cyclogenesis and intensification (Montgomery and Smith 2010). In this view, the separate stages proposed in previous significant studies and reviews (e.g. Frank, 1987; Emanuel 1989;

¹⁰The stretching and thereby amplification of ambient (or system-scale) vorticity by convection by itself does not lead to an increase in the circulation because stretching leads to a contraction in the areal extent of the amplified vorticity (see Haynes and McIntyre 1987).

McBride 1995; Karyampudi and Pierce 2002; Tory and Frank, 2010) are unnecessary.

Another line of research on tropical cyclogenesis emerged from the TEXMEX experiment¹¹. This research emphasized the importance of thermodynamical processes within the so-called “mesoscale convective vortex embryo.” Bister and Emanuel (1997) proposed that the development of a cool, moist environment resulting from stratiform rain serves as the incubation region for the formation of a low-level, warm-core cyclonic vortex. They suggested that sustained precipitation in the stratiform cloud deck together with the evaporation of rain drops below would gradually cool and saturate the layer below cloud base while advecting cyclonic vorticity downwards to the surface. Some questions about the dynamics of this process have been raised by Tory and Montgomery (2006), but the thermodynamical aspects are interesting also and worthy of investigation using the data analysed in section 4.

In the pouch-mean data presented for the three developing storms (Figures 13 and 15), we do not find cooling of air below 10 km in altitude. Rather, *in all cases there is slight warming*.

Figure 17 shows the day-to-day evolution of the system-mean relative humidity for pre-Karl and pre-Matthew. In both disturbances there was no significant change in this quantity below about 3 km, but there was a clear moistening above this level between the first and last flight into the storm. These findings do not provide unequivocal support for the Bister and Emanuel picture described above. For one thing we do not see a progressive increase in low- to mid-troposphere relative humidity in all cases. Furthermore, the moistening that we do see cannot be explained by evaporative cooling as it occurs in the presence of increasing temperature: it occurs also through a significant depth of the atmosphere, not just below cloud base. Of course, there is the issue of the horizontal scale differences between the data gathered during TEXMEX and those collected during PREDICT. The sampling strategy for TEXMEX was focused on the scale of a single mesoscale convective system and its associated mesoscale convective vortex, while that for the PREDICT experiment focused on the broader-scale aspects of genesis.

Influenced by the TEXMEX study, Raymond and Sessions (2007) proposed an alternative model for tropical cyclogenesis that is linked with the gross moist stability of the tropical atmosphere. They investigated the hypothesis that an increase in the gross moist stability would lead to a fundamental change in the vertical profile of convergence for a developing tropical disturbance. To this end, they carried out a series of two-dimensional (zonal-height) cumulus ensemble simulations in the context of the weak temperature gradient approximation without background rotation. The experiments imposed small

¹¹TEXMEX is the acronym for the Tropical Experiment in Mexico, which was conducted in the eastern Pacific basin out of Acapulco, Mexico. This experiment is described more fully in Bister and Emanuel (1997) and Raymond et al. (1998).

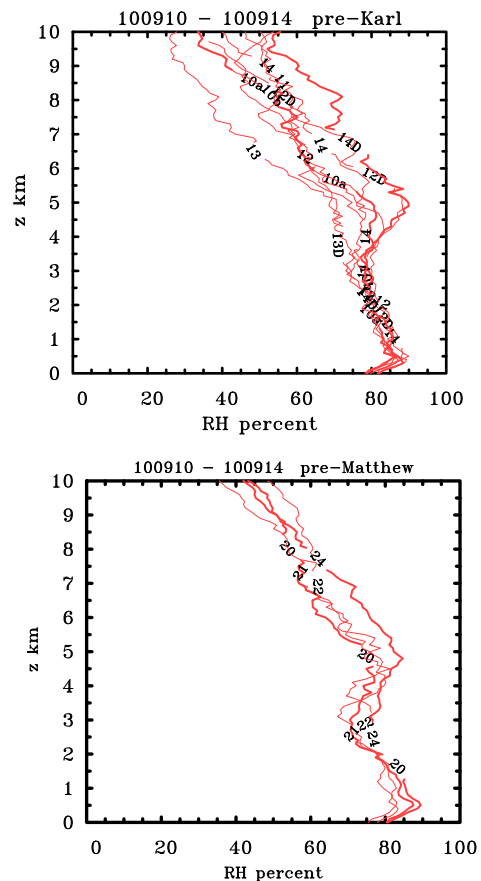


Figure 17. Vertical profiles of departures from mean profiles of system-mean relative humidity on all days for (a) pre-Karl during the period 10–14 September, and (b) pre-Matthew during the period 20–24 September. The thick curves mark the first and last days of the sequence. Numbers on curves refer to the date. A letter ‘D’ refers to a DC-8 flight.

thermal and moisture perturbations to a state of radiative-convective equilibrium as a possible way of investigating the evolution of convection in thermodynamic environments conducive for tropical cyclogenesis. Environments that were cooler at low levels and warmer at upper levels on the order 1 K were found to lower the level of maximum vertical mass flux from 10 km to approximately 5 km; such environments were found to increase the precipitation rate as well. The net result of these effects is to increase the inflow into the convection. The suggestion is that if realistic values of ambient rotation associated with a tropical wave or monsoon trough were included, this inflow would cause a stronger vorticity convergence at lower levels and thus contribute to the spin up of the system. This effect is argued to be an explanation for why tropical-wave-scale mid-level vortices foster tropical storm formation.

While we have several concerns about Raymond and Sessions’ formulation of the problem¹², it is nonetheless

¹²First, the temperature and moisture perturbations imposed in the model are based on observational data taken within a mesoscale convective vortex embryo and proximity soundings of the same mesoscale convective system. It would be fortuitous if these proximity soundings

pertinent to enquire whether there is observational support in the PREDICT data for the configuration envisaged by Raymond and Sessions. As noted above, from the data shown in (Figures 13 and 15), we do not find cooling¹³ of air below 10 km in altitude. Rather, in all developing cases there is slight warming.

While the analyses of CAPE shown here are not useful for distinguishing between developing and non-developing systems, they do indicate significant levels of CAPE in the pouch region of the disturbances analysed. Approximately 50% of soundings had CAPE values exceeding 1500 J kg^{-1} and approximately 10% had values exceeding 2500 J kg^{-1} . This finding is in sharp contrast to the idea conveyed in Emanuel *et al.* (1994) that levels of CAPE over the tropical oceans are minimal, sufficient only to offset the dissipation within clouds. However, we acknowledge that the way in which we define CAPE is different from that of Emanuel *et al.*, who use a definition that assumes reversible adiabatic displacements. Their definition includes the effects of condensed water on air parcel buoyancy and applies to non-precipitating convection. On the basis of our observations we would argue that the levels of CAPE in the pouch region of tropical disturbances are not insignificant and are adequate to support modes of convective organization just as in the middle latitudes over land.

6 Conclusions

This work was carried out to determine the salient thermodynamic characteristics of the ‘‘pouch region’’ of developing and nondeveloping tropical disturbances. To this end we have presented an analysis of the dropwindsonde data obtained for the most extensively documented pre-depression disturbances during the PREDICT, GRIP and IFEX experiments, which were conducted during the peak of the 2010 Atlantic hurricane season. In particular, we describe three cases that were extremely well sampled both spatially and temporally. These data are compared briefly with those of a fully-fledged hurricane obtained during the GRIP portion of the experiment. The analyses provide unprecedented quantitative information about the vertical structure, magnitude, and range of variability of important thermodynamic quantities such as virtual potential temperature and equivalent potential temperature.

were representative of the radiative-convective equilibrium state of the entire tropical disturbance. Indeed, the entire system may not be in a radiative-convective equilibrium state (Brown and Bretherton 1997). These perturbations are treated as perturbations to the radiative convective equilibrium state of the tropical disturbance. Second, the research flights were typically at 700 mb and thus the data obtained were unable to document the convective environment through the troposphere. Third, without ambient rotation and without a truly three-dimensional configuration of the model, these experiments cannot offer insight into the dynamics of the segregation and aggregation of vorticity as discussed above. It is yet to be demonstrated whether the thermodynamic control as envisaged by Raymond and Sessions is essential in a rotational environment.

¹³Although we present fields of virtual potential temperature, the temperature fields exhibit the same day-to-day evolution (not shown).

We calculated the mean sounding of virtual potential temperature and pseudo-equivalent potential temperature on each day for the pouch region of the disturbances. The departures from the system mean averaged over the four or five (mostly consecutive) days of observations was presented also. For the two developing disturbances (Karl and Matthew) in the Caribbean region and for the system that failed to redevelop (ex-Gaston), there was a slight to moderate warming in virtual potential temperature through much of the troposphere during the four or five days of observations, but no obvious change in dry static stability.

Two notable paradigms that have been offered previously to explain tropical cyclogenesis have assumed a modest cooling of the lower troposphere. This presumption is not supported by the PREDICT-GRIP observations.

In contrast to the developing cases, the equivalent potential temperature showed a higher degree of variability in the non-developing ex-Gaston, and even more variability in the case of mature Hurricane Earl. In ex-Gaston, this variability was found to be largely associated with that in the water vapour mixing ratio.

All systems had significant amounts of CAPE, with 50% of soundings having values in excess of 1500 J kg^{-1} and 10% in excess of 2500 J kg^{-1} . Soundings with high values of CAPE tended to have low values of CIN. Interestingly, the largest values ($> 3000 \text{ J kg}^{-1}$) were found in ex-Gaston. These findings are in sharp contrast to the idea conveyed in Emanuel *et al.* (1994) that levels of CAPE over the tropical oceans are minimal, sufficient only to offset the dissipation within clouds. Indeed, it would appear that levels of CAPE in the pouch region of tropical disturbances are not insignificant and are adequate to support modes of convective organization. Even so, the evolution and distribution of CAPE and CIN by themselves did not reveal an obvious distinction between developing and non-developing systems. Perhaps the most potentially significant difference between the developing and non-developing systems was the smaller difference in pseudo-equivalent potential temperature at the surface and the mid-tropospheric minimum of this quantity. This difference was about 15–17 K in the developing systems compared with about 25 K in the non-developing system, ex-Gaston.

These observations provide a context for future study of the interaction between the pouch and its environment and of the development of rotating deep convection within the pouch. Both of these topics are important elements of the marsupial paradigm and research efforts in both directions are currently underway.

7 Acknowledgements

We are grateful to Mark Boothe for providing the consensus pouch tracks, assistance with some of the code checking and for his assistance with finalizing the two figures depicting the GV flight tracks, dropsondes and infrared satellite imagery for the pre-Karl disturbance. We thank also Ed. Zipser and an anonymous reviewer

for their perceptive comments on the original manuscript; and Gerald Thomsen and Gerard Kilroy for their comments on a near final version of the revised version. We acknowledge the United States National Science Foundation for their support of the PREDICT experiment. MTM acknowledges the support of NSF AGS-0733380 and NSF AGS-0851077, NOAA's Hurricane Research Division and NASA grants NNH09AK561 and NNG09HG031. RKS acknowledges financial support for tropical-cyclone research from the German Research Council (Deutsche Forschungsgemeinschaft).

Appendix: Calculation of CAPE and CIN

The values of CAPE and CIN given in this paper are calculated by lifting hypothetical air parcels from the surface and from heights of 100 m - 500 m above the surface at 100 m intervals until the LNB of the particular parcel. Pseudo-adiabatic ascent is assumed and the latent heat of fusion in the upper troposphere is not accounted for. Integrals of the buoyancy force, proportional to the difference between the virtual temperature of a lifted parcel and that of its environment at a given height, are evaluated over the height ranges of positive buoyancy and negative buoyancy using a trapezoidal method with a height interval of 100 m. The sum of the positive and negative integrals for the parcels lifted from 100 m - 500 m is then averaged to give the CAPE. The value of the integral for the parcel lifted from the surface is omitted as, in some cases it can be as much as twice the value at 100 m, calling into question its representativeness. We define the CIN as the minimum value of the six negative integrals (including the surface lifted parcel). The reader is reminded that these methods for calculating CAPE and CIN, like any others, are arbitrary and other methods will give different values. For example, if CAPE is defined solely on the basis of the value for an air parcel lifted from the surface, much larger values may arise.

The calculations use Bolton's formula (Bolton 1980) to evaluate the pseudo-equivalent potential temperature and the formula given in Emanuel (1994, page 116, Eq. 4.4.13) is used to calculate the saturation vapour pressure.

8 References

Bister M Emanuel KA. 1997 The genesis of Hurricane Guillermo: TEXMEX analyses and a modeling study. *Mon. Wea. Rev.*, **125**, 2662-2682.

Bolton D. 1980 The computation of equivalent potential temperature. *Mon. Wea. Rev.*, **108**, 10461053.

Braun SA Montgomery MT Mallen KJ Reasor PD. 2010 Simulation and interpretation of the genesis of Tropical Storm Gert (2005) as part of the NASA Tropical Cloud Systems and Processes Experiment. *J. Atmos. Sci.*, **67**, 999-1025.

Brown RG Bretherton CS. 1997: A test of the strict quasi-equilibrium theory on long time and space scales. *J. Atmos. Sci.*, **54**, 624-638.

Dunkerton TJ Montgomery MT Wang Z. 2009 Tropical cyclogenesis in a tropical wave critical layer: easterly waves. *Atmos. Chem. Phys.*, **9**, 5587-5646.

Elsberry R Harr P. 2008 Tropical cyclone structure (TCS08) Field experiment scientific basis, observational platforms, and strategy. *Asia-Pacific Journal of Atmospheric Sciences*, **44**, 1-23.

Emanuel KA. 1989 The finite amplitude nature of tropical cyclogenesis. *J. Atmos. Sci.*, **46**, 3431-3456.

Emanuel KA. 1994 *Atmospheric convection*. Oxford University Press, 580pp.

Emanuel KA Neelin JD Bretherton CS. 1994 On large-scale circulations in convecting atmospheres. *Q. J. R. Meteorol. Soc.*, **120**, 1111-1143.

Fang J Zhang F. 2010 Initial development and genesis of Hurricane Dolly (2008). *J. Atmos. Sci.*, **67**, 655-672.

Frank WM. 1987: Tropical cyclone formation. In: *A global view of tropical cyclones*. Ed. R. L. Elsberry, Office of Naval Research, 53-90.

Guimond SR Heysmsfield GM and Turk FJ. 2010 Multi-scale observations of Hurricane Dennis (2005): The effects of hot towers on rapid intensification. *J. Atmos. Sci.*, **67**, 633-654.

Halverson J Black M Rogers R Braun S Heysmsfield G Cecil D Goodman M Hood R Heysmsfield A Krishnamurti T McFarquhar G Mahoney MJ Molinari J Turk J Velden C Zhang D-L Zipser E Kakar R. 2007 NASA's Tropical Cloud Systems and Processes Experiment. *Bull. Amer. Meteor. Soc.*, **88**, 867-882.

Haynes P McIntyre ME. On the evolution of vorticity and potential vorticity in the presence of diabatic heating and frictional or other forces. *J. Atmos. Sci.*, **44**, 828-841.

Hendricks EA Montgomery MT Davis CA. 2004 On the role of "vortical" hot towers in formation of tropical cyclone Diana (1984). *J. Atmos. Sci.*, **61**, 1209-1232.

Hiroshi A. 1978 A method of bivariate interpolation and smooth surface fitting for values given at irregularly distributed points. *ACM Transactions on Mathematical Software*, **4**.

Hiroshi A. 1984 On estimating partial derivatives for bivariate interpolation of scattered data. *Rocky Mountain Journal of Mathematics*, **14**.

Holton JR. 2004 *An introduction to dynamic meteorology* Academic Press, London, pp535.

Houze RA. 2004: Mesoscale Convective Systems. *Reviews of Geophysics*, **42**, RG4003, 1-43.

Houze, RA Lee W-C Bell MM. 2009 Convective contribution to the genesis of Hurricane Ophelia (2005). *Mon. Wea. Rev.*, **137**, 2778-2800.

James RP Markowski PM. 2009: A numerical investigation of the effects of dry air aloft on deep convection. *Mon. Wea. Rev.*, **137**, 140-161.

Karyampudi, V. M., and H. F. Pierce, 2002: Synoptic-scale influence of the Saharan air layer on tropical cyclogenesis over the eastern Atlantic. *Mon. Wea. Rev.*, **130**, 3100-3128.

McBride JL. 1995: Tropical cyclone formation. In *Global Perspectives on Tropical Cyclones*. pp21-62. WMO/TD-No 693 (Ed. R. L. Elsberry), World Meteorological Organization, Geneva, 289pp.

Montgomery MT Smith RK. 2010: Tropical-Cyclone Formation: Theory and Idealized modelling. Report for the Seventh International Workshop on Tropical Cyclones, La Réunion, Nov. 2010. World Meteorological Organization, Geneva, Switzerland.

Montgomery MT Smith RK. 2011: Paradigms for tropical-cyclone intensification. Submitted to *Q. J. R. Meteorol. Soc.*,

Montgomery MT Nguyen SV Smith RK. 2009: Do tropical cyclones intensify by WISHE? *Q. J. R. Meteorol. Soc.*, **135**, 1697-1714.

Montgomery MT Davis C Dunkerton T Wang Z Velden C Torn R Majumdar S Zhang F Smith RK Bosart L Bell MM Haase JS Heysmsfield A Jensen JCampos T, Boothe MA. 2011: The Pre-Depression Investigation of Cloud Systems in the Tropics (PREDICT) Experiment: Scientific Basis, New Analysis Tools, and Some First Results. *Bull. Amer. Meteor. Soc.*, in press.

- Nguyen SV Smith RK Montgomery MT. 2008 Tropical-cyclone intensification and predictability in three dimensions. *Q. J. R. Meteorol. Soc.*, **134**, 563-582.
- Ooyama KV. 1969: Numerical simulation of the life cycle of tropical cyclones. *J. Atmos. Sci.*, **26**, 3-40.
- Raymond DJ Sessions SL. 2007: Evolution of convection during tropical cyclogenesis. *Geophys. Res. Lett.*, **34**, L06811, doi:10.1029/2006GL028607
- Reasor PD Montgomery MT Bosart LF. 2005: Mesoscale observations of the genesis of Hurricane Dolly (1996). *J. Atmos. Sci.*, **62**, 3151-3171.
- Ritchie, E. A. and G. J. Holland, 1999: Large-scale patterns associated with tropical cyclogenesis in the western Pacific. *Mon. Wea. Rev.*, **127**, 2027-2043.
- Rutherford B Montgomery MT. 2011: A Lagrangian characterization of a developing and non-developing disturbance observed during the PREDICT Experiment. Submitted to *Atmos. Chem. Phys.*
- Saunders and Montgomery MT. 2004: A closer look at vortical hot towers within a tropical cyclogenesis environment. Colorado State University, Atmospheric Science Bluebook No. 752.
- Shay, LK. 2010: Air-sea interactions. Chapter 42 of Global perspectives on tropical cyclones: From science to mitigation. (Ed. Kepert JD. Chan JCL.) World Scientific Series on Asia-Pacific Weather and Climate, Vol. 4, 448pp.
- Tory KJ Montgomery MT. 2006: Internal influences on tropical cyclone formation. The Sixth WMO International Workshop on Tropical Cyclones (IWTC-VI), San Jos, Costa Rica, 2006. World Meteorological Organization, Geneva, Switzerland.
- Tory K Frank WM. 2010: Tropical cyclone formation. Chapter 2 of Global perspectives on tropical cyclones: From science to mitigation. (Ed. Kepert JD. Chan JCL.) World Scientific Series on Asia-Pacific Weather and Climate, Vol. 4, 448pp.
- Zipser EJ Twohy CH Tsay S-C Hsu NC Heymsfield GM. Lee Thornhill KL Tanelli S Ross R Krishnamurti TN Ji Q Jenkins G Ismail S Ferrare R Chen G Browell EV Anderson B Hood R Goodman HM Heymsfield A Halverson J Dunion JP Douglas M Cifelli R. 2009: The Saharan Air Layer and the fate of African Easterly Waves-NASA's AMMA field study of tropical cyclogenesis. *Bull. Amer. Meteor. Soc.*, **90**, 1137-1156.